Proceedings of ASME FEDSM'00
ASME 2000 Fluids Engineering Division Summer Meeting
Boston, Massachusetts, June 11-15, 2000

FEDSM2000-11015

THE EFFECT OF EXPERIMENTAL FACILITY DYNAMICS ON A CAVITATION INSTABILITY

Mark E. Duttweiler
Div. of Eng. and Applied Science
California Institute of Technology
Pasadena, California, 91125
Email: duttweiler@caltech.edu

Steven E. Schell
Div. of Eng. and Applied Science
California Institute of Technology
Pasadena, California, 91125
Email: schell@caltech.edu

Christopher E. Brennen
Div. of Eng. and Applied Science
California Institute of Technology
Pasadena, California, 91125
Email: brennen@caltech.edu

ABSTRACT

This paper presents the results of an investigation assessing the role experimental facility dynamics might play in determining the nature of a recently observed instability on a cavitating propeller (Duttweiler and Brennen 1999). To address this question, a theoretical model of the facility dynamics is developed. Experiments were conducted to measure the response of the water tunnel facility to volumetric excitations of varying amplitude and frequency, and the measurements are compared with the response predicted by the model. The dynamics of the propeller cavitation are characterized by estimating two parameters (cavitation compliance and mass flow gain factor) previously employed in developing a system transfer function for cavitating pumps (Brennen 1994). Finally, the characteristics of a model for the complete system, incorporating both the cavitating propeller and the experimental facility dynamics, are discussed.

NOMENCLATURE

The following nomenclature is used to denote the various quantities listed below.

A	Cross sectional area.
C	Compliance.
J	Propeller advance ratio, $\pi U/\Omega R$.
K	Non-dimensional cavitation compliance.
K^*	Dimensional cavitation compliance.
L	Inertance.
M	Non-dimensional mass flow gain factor.
M^*	Dimensional mass flow gain factor.
R	Propeller radius.
U	Incoming flow speed.
V	Volume.
Z	Input impedance.
f	Frequency.
g	Gravitational acceleration.
k	Polytropic constant.
m	Mass flow rate.
p	Pressure.
t	Time.
x	Position.
Ω	Propeller angular frequency.
α	Effective angle of attack of propeller blades.
ξ	Cavity volume parameter, $(J_o - J)/\sigma$.
ρ	Density of water.
σ	Propeller cavitation number, $(p_t - p_v)/\frac{1}{2}\rho\Omega^2 R^2$.
ω	Angular frequency.

The following subscripts are used to indicate the location where or the conditions under which the above quantities were measured.

G	Gas above overflow tank free surface.
c	Connecting pipe between tunnel and overflow tank.
cav	Cavitation on propeller.
fs	Free surface of overflow tank.
o	Initial, resonant, or design conditions.
ot	Overflow tank.
p	Piston.

sv Sealed volume of overflow tank.
t Tunnel or tunnel centerline.
v Vapor.
x Propeller cross-section.

INTRODUCTION

A large number of experimental investigations of cavitation (Shen and Peterson 1978; Bark and van Berlekom 1978; Franc and Michel 1988; Kubota et al.1989; Hart et al.1990; McKenney and Brennen 1994; Reisman et al. 1998; Kjeldsen et al. 1999) have focused on the behavior of various unsteady phenomena. Implicitly assumed in many of these investigations is that the phenomena observed within the laboratory facilities accurately reflects the cavitation behavior of devices operating in more open conditions. Relatively little effort (Shen and Peterson 1978) has been made to consider the interactions between the dynamics of the unsteady cavitation and the dynamics of the surrounding experimental facility.

Recent experiments investigating the behavior of a cavitating model Navy propeller (Duttweiler and Brennen 1999) have revealed a cavitation instability characterized by a periodic oscillation in the extent of cavitation both on the propeller blades and in the vortices shed from the propeller blade tips. An explanation for this instability was offered based on insights gained from the partial cavity instability previously observed by several investigators, most notably Wade and Acosta (1966), on two dimensional hydrofoils.

However, questions remain regarding possible interactions between the cavity volume fluctuations and the response of the experimental facility to this volumetric excitation. The current work attempts to explore such interactions. As evidenced by previous investigations (Brennen 1994) into the behavior of cavitating pumps, the interaction of these dynamics can give rise to "active" overall system dynamics that can provide a net flux of energy to the flow, greatly altering the nature of the observed unsteady cavitation phenomena.

FORCED OSCILLATION SETUP

To assess the response of the facility to the cavity volume excitation, tests were conducted in the water tunnel in the absence of cavitation. The output from an oscillating piston was directed into the tunnel test section through a short run of essentially rigid pipe, as shown in Fig. 1. The combination of piston diameter (38 *mm*) and range of oscillation amplitudes ($3.0 - 15.0$ *mm*) was chosen to approximate the change in cavity volume observed throughout the cavitation instability cycle. The range of oscillation frequencies ($0 - 12$ *Hz*) was sufficient to include the typical instability frequency of 10 *Hz* (Duttweiler and Brennen 1999).

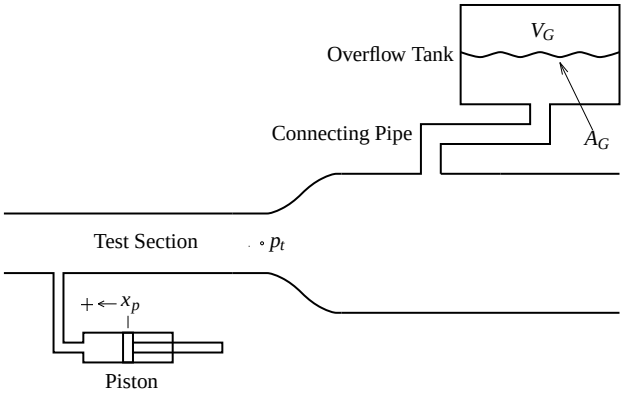

Figure 1. Schematic of the forced oscillation experimental setup.

To ensure that the motion of the piston was as nearly sinusoidal as possible, the pressure of the tunnel test section was adjusted so as to balance the pressures on either side of the oscillating piston. The fluctuations in tunnel test section pressure, p_t, resulting from the piston motion were measured with a pressure transducer mounted at the test section centerline. Cross-correlation software was used to determine both the frequency and amplitude of the pressure oscillations. Furthermore, by monitoring the output from a shaft encoder on the motor driving the oscillating piston, the phase difference between the piston motion and tunnel oscillation was also determined.

MODELING THE FACILITY DYNAMICS

Before considering the results from these forced oscillation experiments, a model will be developed to predict the response of the facility to the piston oscillations. In developing such a model, the facility is assumed to respond in a linear manner to small perturbations in the flow conditions. Accordingly, the quantities of interest are expressed as a linear combination of a mean component and a fluctuating component of frequency ω. The piston position and test section pressure are thus denoted by

$$x_p = \bar{x_p} + \Re[\tilde{x}_p e^{j\omega t}] \quad (1)$$

$$p_t = \bar{p_t} + \Re[\tilde{p}_t e^{j\omega t}], \quad (2)$$

where $\tilde{x}_p$ and $\tilde{p}_t$ are complex and incorporate both the amplitude and phase of the fluctuation.

As can be seen from Fig. 1, the facility dynamics are most simply represented by a parallel combination of a tunnel compliance and the dynamics of the overflow tank (containing the free surface of the water tunnel) and its associated connecting pipe. The overflow tank and connecting pipe dynamics are in turn characterized by a series combination of the connecting pipe inertance and resistance and the compliance of the overflow tank.

Finally, the overflow tank compliance is itself composed of two compliances, one associated with changes in free surface height and the other with the sealed volume of air above the free surface. These dynamic elements combine to give an overall response function, relating $\tilde{x}_p$ to $\tilde{p}_t$, of

$$H(\omega) = \frac{\tilde{p}_t}{\tilde{x}_p} = \frac{\rho A_p \left(\frac{1}{C_{ot}} + j\omega R_c - \omega^2 L_c \right)}{C_t \left[\left(\frac{1}{C_{ot}} + \frac{1}{C_t} \right) + j\omega R_c - \omega^2 L_c \right]}, \qquad (3)$$

where, assuming polytropic behavior of the gas above the free surface, the overflow compliance is given by

$$\frac{1}{C_{ot}} = \frac{1}{C_{fs}} + \frac{1}{C_{sv}} = \frac{1}{\frac{A_G}{g}} + \frac{1}{\frac{\rho V_G}{p_G k}}, \qquad (4)$$

where $\bar{V}_G$ represents the unperturbed volume of air above the free surface and $\bar{p}_G$ the unperturbed pressure of the air. From Eq. 3 it is clear that the tunnel compliance affects the tunnel dynamics more directly than the overflow tank compliance.

DETERMINING PARAMETERS IN THE MODEL

Several of the parameters in the preceding model can be evaluated directly from physical laboratory measurements. From the geometry of the connecting pipe, $R_c = 8.35\ m^{-1}s^{-1}$ and $L_c = 6.02 \times 10^2\ m^{-1}$. Also, for a free surface at the overflow tank midline and atmospheric pressure above the free surface, $C_{fs} = 6.42 \times 10^{-2}\ ms^2$ and $C_{sv} = 1.05 \times 10^{-3}\ ms^2$, yielding a total overflow tank compliance $C_{ot} = 1.03 \times 10^{-3}\ ms^2$.

Remaining to be evaluated, however, is the value of the compliance associated with the expansion and contraction of the tunnel walls, C_t. It is possible to obtain an estimate for this compliance by directly measuring the response of the tunnel walls to changes in internal pressure. Figure 2 shows the deflection of the tunnel at various locations on the exterior of the tunnel.

Five of these locations were on the roughly rectangular test section front panel, which has a length of 125 *cm* and an average height of 32 *cm*. One measurement was obtained precisely at the center of this front panel. Two more measurements were made at the midpoints of the short and long edges of the test section panel, 2.5 *cm* from the surrounding frame. A single measurement was taken in the corner of the test section panel, 2.5 *cm* from both edges of the panel. Finally, a measurement was also taken in the center of the panel located on the backside of the test section.

Three additional measurements were taken on a large metal end wall located downstream of the test section, immediately after the turning vanes direct the flow downward towards the flow return path. This end wall was chosen as representative of the less rigidly reinforced tunnel surfaces. The three measurements were obtained at varying distances from an essentially rigid supporting flange.

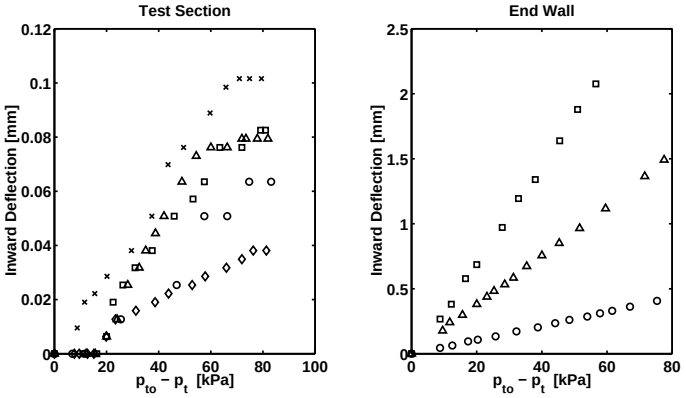

Figure 2. Deflection of tunnel walls in response to a reduction of tunnel pressure p_t below an initial tunnel pressure p_{to}. Left plot shows deflection of test section panels – front panel center (△), front panel short edge midpoint (∘), front panel long edge midpoint (□), front panel corner (◊), and rear panel center (×). Right plot shows deflection of tunnel end wall near downstream turning vanes – 8 *cm* (∘), 22 *cm* (△), and 47 *cm* (□) from the supporting flange.

Figure 2 clearly shows that the amount of deflection varies greatly with location. Not surprisingly, the test section panel, constructed of thick glass and more rigidly supported by its surrounding frame, shows less deflection than the weaker end wall. Also as expected, the measurements taken at locations further from surrounding supports exhibit greater deflection. Exactly why some locations on the test section panel exhibit a delay in the onset of contraction is not understood.

It is probable that other locations throughout the tunnel (where size, shape, and extent of reinforcement, as well as material vary widely) would also show similar variation. Nonetheless, it is possible to estimate very crudely from Fig. 2 a value for the compliance of the tunnel. From the definition of the tunnel compliance

$$C_t \doteq \rho \frac{dV_t}{dp_t} = \rho \frac{dV_t}{dx_t} \frac{dx_t}{dp_t}, \qquad (5)$$

where x_t is the position of a tunnel surface, $\frac{dx_t}{dp_t}$ a slope from Fig. 2, and $\frac{dV_t}{dx_t}$ the surface area of the tunnel. Estimating the tunnel surface area as 75 m^2, a range of

$$7.5 \times 10^{-5}\ ms^2 \leq C_t \leq 1.5 \times 10^{-3}\ ms^2 \qquad (6)$$

is obtained for the tunnel compliance.

NATURAL FREQUENCY EXPERIMENTS

Neglecting the contribution of the connecting pipe resistance, which is insignificant given the parameters determined above, the natural frequency of the response function of Eq. 3 is given by

$$\omega_o \approx \left[\frac{1}{L_c C}\right]^{\frac{1}{2}} = \left[\frac{1}{L_c}\left(\frac{1}{C_t} + \frac{g}{A_G} + \frac{\bar{p}_G k}{\rho V_G}\right)\right]^{\frac{1}{2}}, \qquad (7)$$

where $C^{-1} = C_{ot}^{-1} + C_t^{-1}$ is simply the combined tunnel and overflow tank compliance. The natural frequency is thus a function of the overflow tank conditions through its dependence on C and therefore C_{ot}.

Experiments were conducted to measure this natural frequency at varying $\bar{p}_G$. The tunnel test section pressure was perturbed by the rapid closure of a valve connecting the overflow tank to the vacuum system, and then allowed to oscillate freely. The natural frequency was determined using a cross-correlation method.

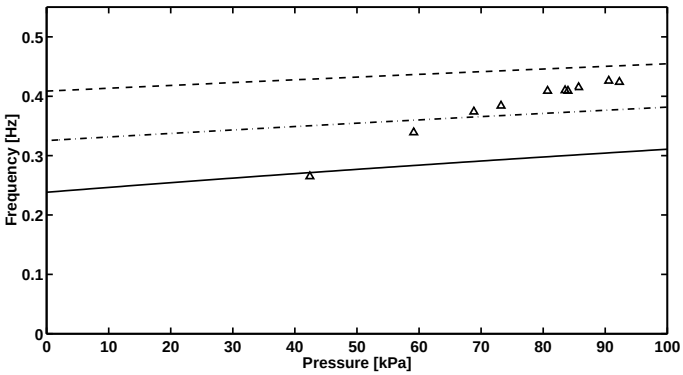

Figure 3. Variation in natural frequency with changing overflow tank pressure. Experimental data (△) and theoretical predictions with overflow tank compliances $C_t = 2.50 \times 10^{-4}$ (−−), 4.00×10^{-4} (· − ·), and $7.50 \times 10^{-4}\ ms^2$ (—).

Figure 3 shows the results of these experiments. The experimentally obtained points are compared with the curves predicted by Eq. 7 using several different values for the tunnel compliance. Readily apparent is the fact that the exact value chosen for the tunnel compliance strongly influences the range of natural frequencies predicted. For a tunnel compliance $C_t = 4.00 \times 10^{-4}\ ms^2$, within the range of Eq. 6, the predicted value of the natural frequency ($f_o \approx 0.4\ Hz$ at $p_t \approx 100\ kPa$), exhibits good agreement with the experimental data. However, the slope of the theoretical curves is substantially less and more nearly constant than that of the experimental data. This seems to indicate that the tunnel compliance may not be constant with varying pressure as suggested by Fig. 2.

FORCED OSCILLATION EXPERIMENTS

To further assess the validity of the proposed model for the facility dynamics, the phase and amplitude of the tunnel pressure oscillations predicted by Eq. 3 can be compared with the results of the previously described forced oscillation experiments. Figure 4 shows both the predicted amplitude for the tunnel compliance of $C_t = 4.00 \times 10^{-4}\ ms^2$ determined from the natural frequency experiments, and the experimentally measured amplitude, over a frequency range near the natural frequency.

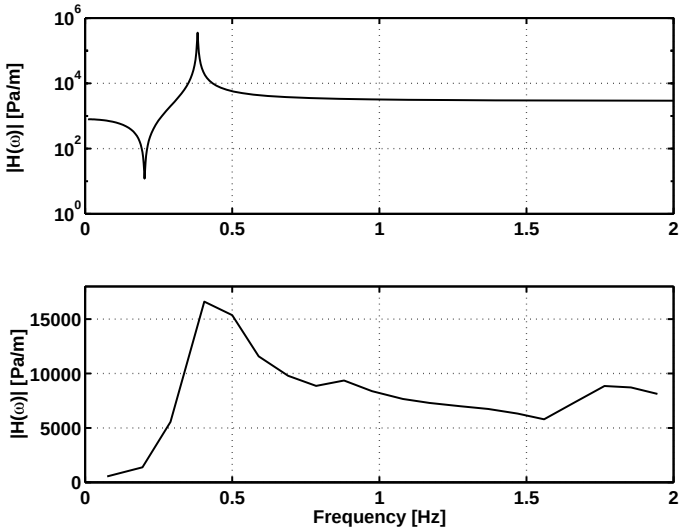

Figure 4. Variation in $|H(\omega)|$ with excitation frequency, near resonance. Upper plot shows the theoretical curve predicted by Eq. 3, lower plot the experimental data.

In general, the theoretically predicted and experimentally obtained amplitudes show good agreement. Both exhibit a resonant peak very near the natural frequency of $f_o \approx 0.4\ Hz$. Furthermore, both show similar values through the range of frequencies above the resonant peak. Not surprisingly, the height of the resonant peak exhibited by the real system is much less than that predicted by the model. It is probable that the physical system contains some additional unmodeled damping. Also, the experimentally obtained resonant peak is much broader than that predicted by the model. This broadening of the peak is likely attributed to the fact that the tunnel compliance is not located at the end of a single, discrete flow path as implied by the model, but rather along a continuous series of flow paths. In this sense,

the physical system would not exhibit a single, well-defined resonance, but rather a range of resonances.

Finally, it is unclear whether the experimental data exhibits the anti-resonant trough predicted by Eq. 3. The resolution in frequency provided by the experiments is not fine enough and the lowest attainable frequencies are not low enough to discern the behavior of the tunnel response in the frequency range ($f = 0.05 - 0.35\,Hz$) where Eq. 3 predicts a minimum in the response.

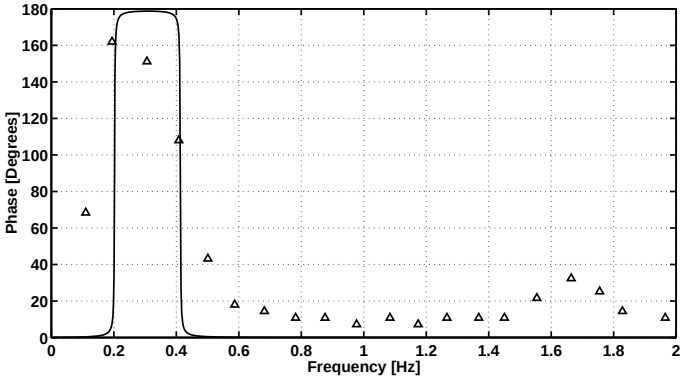

Figure 5. Plot of $ArgH(\omega)$ near resonance. Experimental data (△) and theoretical prediction of Eq. 3 (—).

Figure 5 shows the results of experiments conducted to investigate the phase lag between the piston motion and the tunnel pressure oscillations, as well as the phase predicted by Eq. 3. Again, the experiments were conducted over frequencies ($f = 0.1 - 2.0\,Hz$) near resonance, where the model indicates a dramatic phase transition. The agreement between the experiments and the predictions of the model is good. As expected, though, the physical system exhibits a more poorly defined phase transition near resonance. Somewhat puzzling, though, is the slight increase in phase exhibited by the experimental data through the frequency range of $f = 1.5 - 1.8\,Hz$.

Because the cavitation instability observed in Duttweiler and Brennen (1999) occurred at frequencies near 10 Hz, experiments were also run at higher frequencies ($f = 1 - 12\,Hz$) away from resonance. No additional resonant peaks were found, but rather the response exhibited a steady decay towards higher frequencies. While this seems an appropriate behavior for the physical system, it is in marked contrast to the constant, non-zero response predicted by the model at higher frequencies.

CAVITATION DYNAMICS

The preceding experiments demonstrate that the test section flow conditions will respond to the volumetric excitations imposed by a fluctuating cavity volume in the tunnel test section. Yet, the cavity volume itself responds to changes in the test section flow conditions. Clearly then, the cavitation dynamics and facility dynamics must be considered as part of a coupled system.

Essential to understanding these coupled dynamics is determining how the cavity volume responds to changing inlet conditions. As suggested by Brennen (1995) and Tulin (1953) during studies of two dimensional hydrofoils, the non-dimensional cavity length, $\frac{l}{c}$, is approximately a function of the ratio of the effective angle of attack of the propeller blade to the cavitation number, $\frac{\alpha}{\sigma}$. Furthermore, since as proposed by Blake (1986) the cavity volume is proportional to the propeller radius and the square of the cavity length, the total cavity volume is also essentially a function of the ratio $\frac{\alpha}{\sigma}$.

At a given propeller speed, the effective angle of attack α is determined entirely by the mass flow rate entering the propeller disc, m_x, while the cavitation number is determined entirely by the test section pressure p_t. It is therefore appropriate to express the variation in cavity volume with α and σ in terms of a cavitation compliance $K^* = -\rho(\frac{dV_{cav}}{dp_t})_{m_x}$ and a mass flow gain factor $M^* = -\rho(\frac{dV_{cav}}{dm_x})_{p_t}$ (Brennen 1994). Finally, it is convenient to recast these in terms of parameters more frequently encountered in cavitating propeller experiments, the advance ratio J and the cavitation number σ.

$$K^* \doteq -\rho\left(\frac{dV_{cav}}{dp_t}\right)_{m_x} = -\frac{2}{\Omega^2 R^2}\left(\frac{dV_{cav}}{d\sigma}\right)_J \tag{8}$$

$$M^* \doteq -\rho\left(\frac{dV_{cav}}{dm_x}\right)_{p_t} = -\frac{\pi}{A_x \Omega R}\left(\frac{dV_{cav}}{dJ}\right)_\sigma, \tag{9}$$

where Ω is the angular frequency of the propeller, R the radius of the propeller, and A_x the propeller frontal area.

Equations 8 and 9 demonstrate that it is possible to determine values for K^* and M^* from experiments determining cavity volume at varying J and σ. Figure 6 shows the results from such a set of experiments. Here, the cavity volume was calculated by combining the method proposed by Blake (1986) with direct observation of the cavity length.

Some insight into these variations in cavity volume can be gained by considering that, based on geometry, the effective angle of attack of a propeller blade, α, is approximately proportional to the difference between the design and operating advance ratios, $J_o - J$. Then, from the preceding arguments, the cavity volume is essentially a function of the parameter $\xi = (J_o - J)/\sigma$, with a constant value corresponding to a constant cavity volume. Accordingly, several lines of constant ξ are plotted in Fig. 6.

Given the good correspondence between lines of constant ξ and the experimentally determined contours of constant volume, it is convenient to fit the cavity volume to a function of the form $V_{cav} = h(\xi)$. Choosing a second order polynomial $h(\xi) = a\xi^2 +$

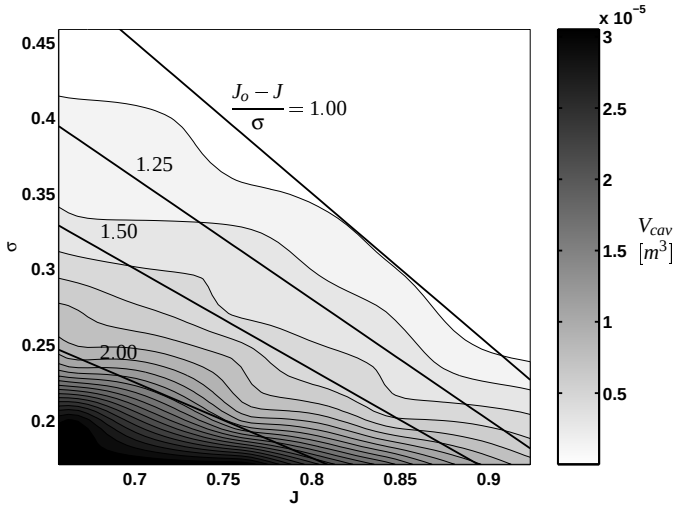

Figure 6. Total cavitation volume as a function of advance ratio and cavitation number. Propeller operating at $1700\ RPM$.

$b\xi + c$, Eqs. 8 and 9 yield

$$K^* = \frac{2}{\Omega^2 R^2 \sigma}(2a\xi^2 + b\xi) \tag{10}$$

$$M^* = \frac{\pi}{A_x \Omega R \sigma}(2a\xi + b), \tag{11}$$

where $a = 0.86 \times 10^{-5}\ m^3$ and $b = -1.2 \times 10^{-5}\ m^3$. Appropriately non-dimensionalized, Eqs. 10 and 11 yield values for the dimensionless cavitation compliance and dimensionless mass flow gain factor of $K \doteq \frac{K^*\Omega^2}{R} = 0.2 - 0.8$ and $M \doteq M^*\Omega = 0.05 - 0.20$ at $\sigma = 0.2$, over the range of advance ratios investigated.

These values can be compared with those obtained by previous investigators for cavitating pumps. For example, in the first theoretical calculation of these dynamic parameters for a cavitating inducer, Brennen and Acosta (1976) obtained values in the ranges $K = 0.05 \rightarrow 0.2$ and $M = 0.6 \rightarrow 0.8$ for cavitation numbers above $\sigma = 0.02$. Experimental measurements by Brennen et al. (1982) for cavitating inducers led to a larger typical value of $K \approx 0.25$, but similar values of $M \approx 0.6$ at $\sigma = 0.2$. More recently, Otsuka et al. (1996) examined theoretically the potential frequency dependence of K and M. At low frequency they obtained values of the order of $K \approx 0.06$ and $M \approx 0.6$ at $\sigma = 0.17$. These values offer reasonable agreement with those determined in the current work given the substantial differences between propeller and pump geometries.

CAVITATION AND FACILITY DYNAMICS INTERACTION

Recent work investigating the unsteady performance of cavitating pumps (Brennen and Acosta 1976; Brennen 1978; Brennen et al. 1982; Otsuka et al. 1996) has documented the importance of the cavitation compliance and mass flow gain factor in determining the stability of a system containing a cavitating pump. This can be illustrated by considering a very simplistic system including only the cavitation and mass flow gain factor. Then, if the discharge impedance from the pump is infinite, the input impedance, $Z = \frac{\tilde{p}_t}{\tilde{m}_t}$, has a real part given by

$$\Re[Z] = -\frac{M^*}{K^*}, \tag{12}$$

where a negative value of $\Re[Z]$ implies a source of fluctuation energy.

Therefore, in a similar manner, the positive values obtained for K^* and M^* imply that the cavitating propeller is potentially capable of sustaining an instability in the surrounding facility. Of course, any frictional resistance in the facility will tend to counteract and perhaps outweigh this effect. Moreover, if the facility dynamics were added to provide a complete model of the system dynamics, the system stability would become frequency dependent. It seems likely that specific frequency ranges would emerge as the most unstable. Thus, although the basic cavitation model does not indicate a particular instability frequency, the coupling with the facility dynamics should do so. Research is continuing to investigate possible methods of completing this model.

CONCLUSIONS

In an effort to better understand the origins of a recently observed instability on a cavitating propeller, potential interactions between the cavitation and facility dynamics have been considered. First, a model was developed for the dynamics of the water tunnel facility. The proposed model illustrates the important role played by the tunnel compliance in determining the facility dynamics. Utilizing a value for this compliance estimated from direct measurements of the response of the tunnel to changing internal pressures, good agreement was obtained between the experimentally observed and theoretically predicted natural frequency, amplitude of response, and phase of response.

Also, values were determined for the cavitation compliance and mass flow gain factor from experiments measuring the cavity volume at varying inflow conditions. The values obtained in this manner offered reasonable agreement with those obtained for cavitating pumps. Most importantly, the values of these two parameters suggest that the previously observed instability might be predicted by a model incorporating both the facility and cavitation dynamics.

ACKNOWLEDGEMENTS

The authors would like to acknowledge the Office of Naval Research and technical monitor Dr. Edwin Rood for their generous support of this research. The research program was funded under Contract N00014-97-1-0002. Finally, Dr. Teiichi Tanaka provided much assistance in conducting the tunnel response experiments.

REFERENCES

Bark, G. and W. van Berlekom, 1978, Experimental investigations of cavitation noise, *Proc. 12th ONR Symp. on Naval Hydrodynamics*, pp. 470–493.

Blake, W. K., 1986, Propeller cavitation noise: the problems of scaling and prediction, *ASME Proc. Int. Symp. on Cavitation and Multiphase Flow Noise*, Vol. FED 45, pp. 89–100.

Brennen, C. E., 1978, Bubbly flow model for the dynamic characteristics of cavitating pumps, *J. of Fluid Mech.*, Vol. 89, pp. 223–240.

Brennen, C. E., 1994, *Hydrodynamics of Pumps*, Concept ETI and Oxford Univ. Press.

Brennen, C. E., 1995, *Cavitation and Bubble Dynamics*, Oxford Univ. Press.

Brennen, C. E. and A. J. Acosta, 1976, The dynamic transfer function for a cavitating inducer, *ASME J. of Fluids Eng.*, Vol. 98, pp. 182–191.

Brennen, C. E., C. Meissner, E. Y. Lo, and G. S. Hoffman, 1982, Scale effects in the dynamic transfer functions for cavitating inducers, *ASME J. of Fluids Eng.*, Vol. 104, pp. 428–433.

Duttweiler, M. E. and C. E. Brennen, 1999, Experimental investigation of an instability on a cavitating propeller, *Proc. ASME Cavitation and Multiphase Flow Forum*.

Franc, J. P. and J. M. Michel, 1988, Unsteady attached cavitation on an oscillating hydrofoil, *J. of Fluid Mech.*, Vol. 193, pp. 171–189.

Hart, D. P., C. E. Brennen, and A. J. Acosta, 1990, Observations of cavitation on a three dimensional oscillating hydrofoil, *Proc. ASME Cavitation and Multiphase Flow Forum*, Vol. FED 98, pp. 49–52.

Kjeldsen, M., R. E. A. Arndt, and M. Effertz, 1999, Investigation of unsteady cavitation phenomenon, *Proc. ASME Cavitation and Multiphase Flow Forum*.

Kubota, A., H. Kato, H. Yamaguchi, and M. Maeda, 1989, Unsteady structure measurement of cloud cavitation on a foil section using conditional sampling, *ASME J. of Fluids Eng.*, Vol. 111, pp. 204–210.

McKenney, E. A. and C. E. Brennen, 1994, On the dynamics and acoustics of cloud cavitation on an oscillating hydrofoil, *Proc. ASME Symp. on Cavitation and Gas-Liquid Flows in Fluid Machinery and Devices*, Vol. FED 190, pp. 195–202.

Otsuka, S., Y. Tsujimoto, K. Kamijo, and O. Furuya, 1996, Frequency dependence of mass flow gain factor and cavitation compliance of cavitating inducers, *ASME J. of Fluids Eng.*, Vol. 118, pp. 400–408.

Reisman, G. E., Y.-C. Wang, and C. E. Brennen, 1998, Observations of shock waves in cloud cavitation, *J. of Fluid Mech.*, Vol. 355, pp. 255–283.

Shen, Y. and F. B. Peterson, 1978, Unsteady cavitation on an oscillating hydrofoil, *Proc. 12th ONR Symp. on Naval Hydrodynamics*, pp. 362–384.

Tulin, M. P., 1953, Steady two-dimensional cavity flows about slender bodies, Technical Report 834, David Taylor Model Basin.

Wade, R. B. and A. J. Acosta, 1966, Experimental observations on the flow past a plano-convex hydrofoil, *ASME J. of Basic Eng.*, Vol. 88, pp. 273–283.